Nonlinear Theory of Parametric Oscillator: Steady-State Operation and Fluctuation Analysis

ROBERTO CAZZOLA, GIANPIERO P. PONCINO, ELIO BAVA, ALDO GODONE, AND GIAN PAOLO BAVA

Abstract—**Parametric oscillators with a superconducting output cavity are of great interest as sources of very high frequency stability. In this paper, a careful analysis is performed for a parametric oscillator model based on an abrupt junction varactor with fixed-bias voltage and ideal shunt mode operation. Steady-state operation, transfer functions for amplitude and phase fluctuations, and additive noise contributions are examined. An overall estimation of system performance as regards to the phase instabilities shows that, although the foreseen characteristics are less outstanding than expected from a previously reported analysis, this device compares favorably with the most important available sources based on atomic transitions or on superconducting cavity-stabilized oscillators.**

I. Introduction

MICROWAVE OSCILLATORS, locked to superconducting cavities, have reached very good stability performance in the short and medium term [1], [2] ($\sigma_y \sim 10^{-15}$ in the time interval 10–1000 s), useful in several fields such as frequency and time metrology, and very long baseline interferometry (VLBI). However, in some applications, mainly for fundamental physical research, sources with improved stability would be highly desirable. To achieve this goal, parametric oscillators with a superconducting output cavity have been proposed as good candidates on the basis of theoretical evaluations [2], [3]. The foreseen performance is based on a rather simple analysis of the parametric oscillator [4] and accounts for thermal noise only. Since these devices behave in a more complex way than the usual negative resistance oscillator and are affected by several noise sources of different origin, a more accurate investigation of the steady-state operation and of the influence of noise seems useful. According to this analysis, the parametric oscillator still appears the most promising microwave source as regards medium-term stability, though with performance less outstanding than that anticipated. This result is mainly due to the transfer of pump amplitude noise to the output phase fluctuation, which turns out to be the most important instability contribution. The thermal noise, though negligible, is mainly generated in the idler mesh.

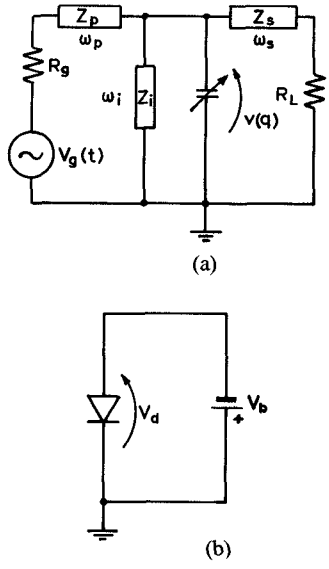

Fig. 1. (a) RF equivalent circuit of the oscillator. (b) Bias network. Varactor parasitic parameters included in Z_p, Z_i, Z_s.

In the present paper, after the statement of the model adopted for the oscillator, the nonlinear analysis of steady-state operation is carried out. A design procedure for maximum efficiency is analytically developed; deviations from the optimum condition, fluctuations transfer, and internal noise contributions are analyzed with the aid of a numerical computation. A general performance evaluation of an *X*-band oscillator, as regards the phase and amplitude stability, is reported.

II. Parametric Oscillator Model

In this section, a parametric oscillator, using a varactor in "shunt diode" mode configuration is considered. The equivalent circuit is shown in Fig. 1, where subscripts p, i, and s refer to the pump, idler, and signal meshes, respectively. The corresponding angular frequencies $\omega_p, \omega_i, \omega_s$

Manuscript received January 25, 1983; revised May 2, 1983. This work was supported by the Consiglio Nazionale delle Ricerche of Italy.

R. Cazzola and G. P. Poncino are post-graduate guest workers, Istituto Elettrotecnio Nazionale Galileo Ferraris, Torino, Italy.

E. Bava and A. Godone are with the Istituto Elettrotecnio Nazionale Galileo Ferraris, Torino, Italy.

G. P. Bava is with the Istituto di Elettronica e Telecomunicazioni, Politecnico di Torino, Italy.

0018-9480/83/1000-0797$01.00 ©1983 IEEE

satisfy the relation $\omega_p = \omega_i + \omega_s$. The subsequent analysis is based on the following assumptions, most of which are commonly adopted in the theory of varactor frequency multipliers and parametric amplifiers [4]–[7].

1) The varactor parasitic parameters (series inductance and resistance) are included in Z_n ($n = p, i, s$).

2) The impedances Z_n have filtering characteristics so as to allow the current flow only in a narrow band around the corresponding resonance frequencies.

3) The detailed calculations are carried out for an abrupt-junction varactor characteristic $v(q)$.

4) In order to simplify the analytical expressions, ω_s and ω_i will be assumed to satisfy the inequalities: $\omega_s \neq \omega_i$, $\omega_s \neq 2\omega_i$, $\omega_i \neq 2\omega_s$; however, some results for the degenerate case $\omega_i = \omega_s$ (two meshes frequency divider) will also be reported in Appendix I.

5) Only fixed-bias varactor operation is considered.

6) As regards the analysis of fluctuations (Section IV), the impedances $Z_n = R'_n + jX_n$ are represented by simple series-resonant circuits (R'_n, L_n, C_n).

The mathematical formalism in the following will be essentially the same as that adopted in [5], except that now the working frequencies are not harmonically related. Therefore, the details of the analysis will not be completely reported here.

The second assumption allows expressing the varactor charge q as follows:

$$q = q_0 + Q'_p + Q'_i + Q'_s \tag{1}$$

when q_0 is the average charge value

$$Q'_n = q_n(t)\sin[\omega_n t + \varphi_n(t)]$$

and the amplitude and phase fluctuations $q_n(t)$ and $\varphi_n(t)$ are supposed to be slowly varying time functions.

According to assumption (6), the voltage V_n across Z_n is

$$\begin{aligned} V_n(t) = {} & \left\{\left(R'_n q_n + 2L_n\frac{dq_n}{dt}\right)\left(\omega_n + \frac{d\varphi_n}{dt}\right) + L_n q_n \frac{d^2\varphi_n}{dt^2}\right\} \\ & \cdot\cos(\omega_n t + \varphi_n) + \left\{R'_n\frac{dq_n}{dt} + L_n\frac{d^2q_n}{dt^2} - L_n q_n \right. \\ & \left.\cdot\left(\omega_n + \frac{d\varphi_n}{dt}\right)^2 + \frac{q_n}{C_n}\right\} \\ & \cdot\sin(\omega_n t + \varphi_n). \end{aligned} \tag{2}$$

After separating the in-phase and quadrature components in the mesh equations for the circuit of Fig. 1, the following system is obtained:

$$\left(R_s q_s + 2L_s\frac{dq_s}{dt}\right)\left(\omega_s + \frac{d\varphi_s}{dt}\right) + L_s q_s\frac{d^2\varphi_s}{dt^2} + F_c^s(t) = E_c^s(t) \tag{3a}$$

$$R_s\frac{dq_s}{dt} + L_s\frac{d^2q_s}{dt^2} - L_s q_s\left(\omega_s + \frac{d\varphi_s}{dt}\right)^2 + \frac{q_s}{C_s} + F_s^s(t) = E_s^s(t) \tag{3b}$$

$$\left(R_i q_i + 2L_i\frac{dq_i}{dt}\right)\left(\omega_i + \frac{d\varphi_i}{dt}\right) + L_i q_i\frac{d^2\varphi_i}{dt^2} + F_c^i(t) = E_c^i(t) \tag{3c}$$

$$R_i\frac{dq_i}{dt} + L_i\frac{d^2q_i}{dt^2} - L_i q_i\left(\omega_i + \frac{d\varphi_i}{dt}\right)^2 + \frac{q_i}{C_i} + F_s^i(t) = E_s^i(t) \tag{3d}$$

$$\left(R_p q_p + 2L_p\frac{dq_p}{dt}\right)\left(\omega_p + \frac{d\varphi_p}{dt}\right) + L_p q_p\frac{d^2\varphi_p}{dt^2} + F_c^p(t) = v_g\cos(\varphi_p - \varphi_g) + E_c^p(t) \tag{3e}$$

$$R_p\frac{dq_p}{dt} + L_p\frac{d^2q_p}{dt^2} - L_p q_p\left(\omega_p + \frac{d\varphi_p}{dt}\right)^2 + \frac{q_p}{C_p} + F_s^p(t) = v_g\sin(\varphi_p - \varphi_g) + E_s^p(t) \tag{3f}$$

where

$$R_s = R_L + R'_s$$

$$R_p = R_g + R'_p$$

$$F_c^n(t) = \frac{2}{T_0}\int_{t-T_0}^{t} v(q)\cos(\omega_n t' + \varphi_n)\,dt'$$

$$F_s^n(t) = \frac{2}{T_0}\int_{t-T_0}^{t} v(q)\sin(\omega_n t' + \varphi_n)\,dt'$$

$$E_c^n(t) = \frac{2}{T_0}\int_{t-T_0}^{t} e_n(t')\cos(\omega_n t' + \varphi_n)\,dt'$$

$$E_s^n(t) = \frac{2}{T_0}\int_{t-T_0}^{t} e_n(t')\sin(\omega_n t' + \varphi_n)\,dt'$$

and $e_n(t')$ are the internal equivalent noise sources. The noise generators $E_c^n(t)$ and $E_s^n(t)$ can be shown to have a white power spectral density with the value $2\cdot\overline{e_n^2}$ [8].

The pump generator voltage is written as

$$V_g(t) = v_g(t)\cos(\omega_p t + \varphi_g(t))$$

and the integration period T_0 is the common minimum period corresponding to the three frequencies of interest, assumed in rational ratios.

According to assumption (3), the varactor characteristic is given by

$$v(q) = V_0 - mq^2, \qquad m = \frac{1}{4V_0C_0^2} \tag{4}$$

where V is the contact potential and C_0 is the zero-bias capacitance.

By taking into account the inequalities of the assumption (4) and by using the expressions (1) and (4) in the integrals giving F_c^n and F_s^n, we have

$$F_c^s = -mq_i q_p\cos(\varphi_p - \varphi_s - \varphi_i) \tag{5a}$$

$$F_s^s = -2mq_0 q_s + mq_i q_p\sin(\varphi_p - \varphi_s - \varphi_i) \tag{5b}$$

$$F_c^i = -mq_s q_p\cos(\varphi_p - \varphi_s - \varphi_i) \tag{5c}$$

$$F_s^i = -2mq_0 q_i + mq_s q_p\sin(\varphi_p - \varphi_s - \varphi_i) \tag{5d}$$

$$F_c^p = mq_sq_i\cos(\varphi_p - \varphi_s - \varphi_i) \tag{5e}$$

$$F_s^p = -2mq_0q_p + mq_sq_i\sin(\varphi_p - \varphi_s - \varphi_i). \tag{5f}$$

If V_b is the bias voltage produced by an ideal generator

$$V_b = -V_d = -V_0 + m\overline{q^2} = -V_0 + m\left(q_0^2 + \frac{q_s^2 + q_i^2 + q_p^2}{2}\right). \tag{6}$$

Equations (3) and (5) are used in the following sections as starting points for evaluating the stationary-state operation $\left(\text{all } \frac{d}{dt} = 0\right)$ and for studying the oscillator fluctuations induced by the circuit noise sources.

III. Steady-State Operation

The steady-state operation of the oscillator can be analyzed by using system (3), when the condition $d/dt = 0$ is set and terms induced by noise fluctuations are disregarded.

Recalling (5), the following set of equations is obtained:

$$R_s\omega_sq_s - mq_iq_p\cos\psi_0 = 0 \tag{7a}$$

$$-X_s\omega_sq_s - 2mq_0q_s + mq_iq_p\sin\psi_0 = 0 \tag{7b}$$

$$R_i\omega_iq_i - mq_sq_p\cos\psi_0 = 0 \tag{7c}$$

$$-X_i\omega_iq_i - 2mq_0q_i + mq_sq_p\sin\psi_0 = 0 \tag{7d}$$

$$R_p\omega_pq_p + mq_sq_i\cos\psi_0 = v_g\cos\varphi_0 \tag{7e}$$

$$-X_p\omega_pq_p - 2m_0q_p + mq_sq_i\sin\psi_0 = v_g\sin\varphi_0 \tag{7f}$$

where

$$\psi_0 = \varphi_p - \varphi_i - \varphi_s \qquad \varphi_0 = \varphi_p - \varphi_g.$$

Obviously, to get a complete solution to the stationary problem, one must consider the bias equation too, as given in (6).

In order to excite parametric oscillations, the pumping conditions must provide equivalent negative resistances in the signal and idler meshes so as to equal all circuit losses. This leads to the threshold value for the pump power as will be found later.

A. Maximum-Efficiency Operation

The oscillator operation not only depends on the pumping conditions, but also on the circuit parameters. In this section, the circuit design is performed by maximizing the efficiency of the pump-signal power transfer. Details of this computations are given in Appendix I; the most important results are summarized here below.

The signal and idler operating frequencies for given ω_p and filters characteristics, can be obtained by solving the equations

$$X_s\omega_s = X_i\omega_i = X_p\omega_p. \tag{8a}$$

Moreover, the average charge in the diode is given by

$$q_0 = -\frac{X_n\omega_n}{2m}. \tag{8b}$$

Thus from (8b), q_0 being a negative quantity, it can be inferred that all the reactances X_n have to be inductive, as expected since the diode capacitive reactance has to be tuned out.

The maximum value of the efficiency $\eta_{\max}$ is then

$$\eta_{\max} = \frac{\omega_s}{\omega_p}(1-\sqrt{k})^2 \tag{9}$$

where

$$k = \frac{\omega_s\omega_i\omega_p^2}{2m^2P_{\text{av}}}R_i'R_s'R_p'. \tag{10}$$

R_i', R_s', R_p' are the loss resistances in the three meshes, and P_{av} is the available pump power. $\eta_{\max}$ is a decreasing function of k, that is, increases with the pump power; its limiting value is ω_s/ω_p, as it is well known from the Manley–Rowe relationships.

The optimum generator and load resistances are given by

$$\frac{R_g}{R_p'} = \frac{1}{\sqrt{k}} \tag{11a}$$

$$\frac{R_L}{R_s'} = \frac{1}{\sqrt{k}} - 1. \tag{11b}$$

Since in (9) and (11) it must be $k \leqslant 1$, the threshold available pump power turns out as

$$P_{\text{th}} = \frac{\omega_s\omega_i\omega_p^2}{2m^2}R_s'R_i'R_p'. \tag{12}$$

This relation implies that for some definite frequencies, diode characteristics, and internal losses, the circuit design cannot be performed for values of P_{av} lower than the corresponding P_{th}. The threshold power obviously decreases with the loss resistances, as well as for ω_s approaching ω_p.

Finally, one has to take into account that in order to accomplish the maximum efficiency conditions, a proper choice of the fixed-bias voltage is necessary, as it follows from (6), (8b), and (A 5).

B. Effects of Pump Power, Pump Frequency, and Bias Changes

It is worthwhile to examine the parametric oscillator operation under conditions different from that of maximum efficiency, in particular with respect to variations of pump power P_{av}, bias voltage V_b, and pump frequency f_p.

This analysis is of some interest at least as regards the noise behavior of the oscillator, as it will be seen in this section and Section V.

For the numerical calculations, the values of circuit parameters of Table I are assumed. They have been chosen in view of an application to a highly stable microwave oscillator using a superconducting output cavity, and follow from the design criterion outlined in Section III-B.

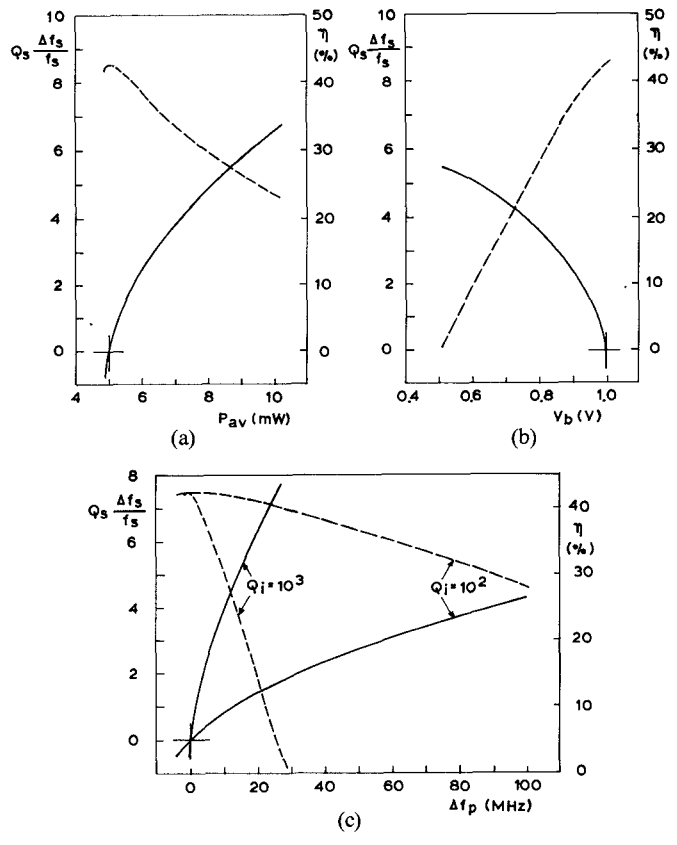

Fig. 2. Normalized signal frequency variations $Q_s \Delta f_s / f_s$ and efficiency η in the limit $Q_s \gg Q_i$ as a function of: (a) P_{av} ($f_p = 20$ GHz, $V_b = 1$ V), (b) V_b ($f_p = 20$ GHz, $P_{av} = 5$ mW), and (c) Δf_p ($P_{av} = 5$ mW, $V_b = 1$ V). Continuous lines = $Q_s \Delta f_s / f_s$; dashed lines = η.

TABLE I
CIRCUIT VALUES AND STATIC PARAMETERS OF THE ANALYZED PARAMETRIC OSCILLATOR

$R_g[\Omega]$	$R_L[\Omega]$	$V_{bopt.}[V]$	$\eta_{MAX.}$ [%]	$X_p[\Omega]$	$X_i[\Omega]$	$X_s[\Omega]$
8.286	7.286	1	42.5	13.667	30.369	24.847

$m = 6.51 \cdot 10^{23}$
$V_0 = 0.6$ [V]
$R'_s = R'_i = R'_p = 1\,\Omega$
$f_p = 20$ GHz
$f_s = 11$ GHz
$P_{av.} = 5$ mW

This means that the circuit parameters of Table I ensure the maximum efficiency operation of the oscillator at $f_s = 11$ GHz for $P_{av} = 5$ mW, and $f_p = 20$ GHz.

If the bias voltage and the pump power and frequency are changed from the values assumed for the circuit design, the quantities of interest can be calculated by solving the system formed by (6) and (7), keeping R_g, R_L, and filter characteristics constant.

The numerical results have been obtained by means of the Newton–Raphson iteration method in matrix form, which is well suited for nonlinear systems [9].

Typical results of the changes in the efficiency η (which is given now by the general expression (A-1)) and the output frequency Δf_s, due to variations in P_{av}, V_b, and f_p are shown in Fig. 2(a), (b), and (c) where

$$Q_n = \frac{\omega_{n0} L_n}{R'_n}, \qquad \omega_{n0} = \frac{1}{\sqrt{L_n C_n}}, \qquad n = p, i, s.$$

At varying P_{av}, V_b, and f_p the parametric oscillation is possible only in a limited range of these "input" quantities, whose extreme values are clearly seen in Fig. 2(b), while only the lower values are reported in Fig. 2(a) and (c). In each case, the operation with η_{max} is very close to one of the limit values which can be interpreted as effective threshold conditions. As a consequence, one must expect that this point is critical.

The y-axis normalization of Fig. 2 yields a very good and significant fit to the obtained numerical results when $Q_s \gg Q_i$ (relative errors less than 1 percent for $Q_s/Q_i \gtrsim 1000$ are presumed). In this case, as regards pump power and bias voltage variations, the output frequency and efficiency variations appear rather insensitive to the magnitude of Q_i.

On the contrary, Fig. 2(c) shows a strong dependence of Δf_s and η on the magnitude of the idler quality factor. Anyway, the effect of Δf_p can be expressed, in accordance with computations on system (7) and in the limit $Q_s \gg Q_i$, as

$$\Delta f_s \simeq \frac{R_s}{R_i} \frac{R'_i}{R'_s} \frac{Q_i}{Q_s} \Delta f_p. \tag{13}$$

IV. Fluctuations in a Parametric Oscillator

Noise effects in a parametric oscillator are already included in (3) and (6), however, this system can be linearized assuming that pump amplitude and phase fluctuations Δv_g and $\Delta\varphi_g$, respectively, are very small, that is $|\Delta v_g| \ll v_{g0}$ and $|\Delta\varphi_g| \ll 1$ rad. Similar conditions are considered for the thermal noise equivalent generators in the three meshes. The linearized system is reported in Appendix II as equations from (A-1) to (AI-7). The unknowns are Δq_p, Δq_i, Δq_s, $\Delta\varphi_p$, $\Delta\varphi_i$, $\Delta\varphi_s$, Δq_0 which represent the complex amplitudes of the deviations from the static values q_p. q_i, q_s, φ_p, φ_i, φ_s, q_0 while v_{g0} and V_{b0} are the mean pump amplitude and dc bias, respectively. Ω in Appendix II is the Fourier angular frequency of fluctuations.

Typical results of numerical computations are analyzed in the following. Four cases are considered and the corresponding static values are reported in Table II. A' and A'' data refer to the maximum efficiency condition previously considered, but with two different values of Q_i; B and C data correspond to two nonoptimum situations.

The effects of pump fluctuations on the output signal are shown in Figs. 3 and 4 as a function of Ω/ω_s. In Fig. 3, the amplitude-to-frequency (AM–FM) and phase-to-phase (PM–PM) transfer functions are given. The curves appear rather flat at a value corresponding to the static perturbation limit; a small variation occurs at the signal resonator bandwidth limit while the effect of the idler resonator is more pronounced. In Fig. 4, the amplitude-to-amplitude

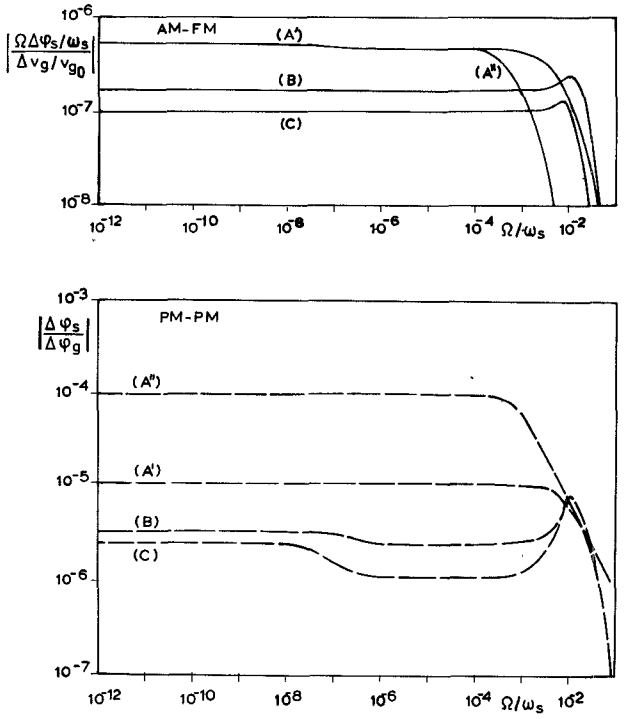

Fig. 3. AM–FM transfer function modulus ($|\Omega \Delta\varphi_s/\omega_s/\Delta v_g/v_{g0}|$) and PM–PM transfer function modulus ($|\Delta\varphi_s/\Delta\varphi_g|$). Continuous lines = AM–FM; dashed lines = PM–PM.

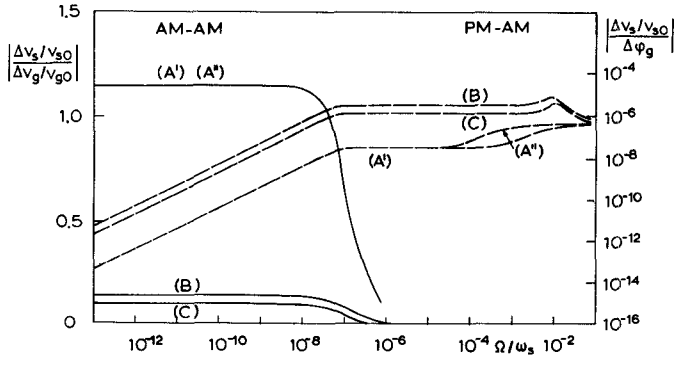

Fig. 4. AM–AM transfer function modulus ($|\Delta v_s/v_{s0}/\Delta v_g/v_{g0}|$) and PM–AM transfer function modulus ($|\Delta v_s/v_{s0}/\Delta\varphi g|$). Continuous lines = AM–AM; dashed lines = PM–AM.

TABLE II
STATIC VALUES OF THE ANALYZED PARAMETRIC OSCILLATOR PARAMETERS

CASE	P_{RF} [mW]	V_b [V]	Q_i	$q_0 \cdot 10^{-12}$ [c]	$q_p \cdot 10^{-12}$ [c]	$q_i \cdot 10^{-12}$ [c]	$q_s \cdot 10^{-12}$ [c]	φ_0 (o)	φ_0 (o)
A'	5	1	10^2	- 1.3190	0.2764	1.1124	0.3495	0	0
A"	5	1	10^3						
B	7	1	10^2	- 1.2747	0.3948	1.1723	0.3684	45.56	15.14
C	5	0.7	10^2	- 1.2673	0.4297	0.7372	0.2316	49.96	5.60

$f_p = 20$ GHz, $f_s = 11$ GHz, $Q_s = 10^8$.

(AM–AM) and phase-to-amplitude (PM–AM) diagrams are reported. As regards the AM–AM curves for the maximum efficiency operation, the static limit can be also

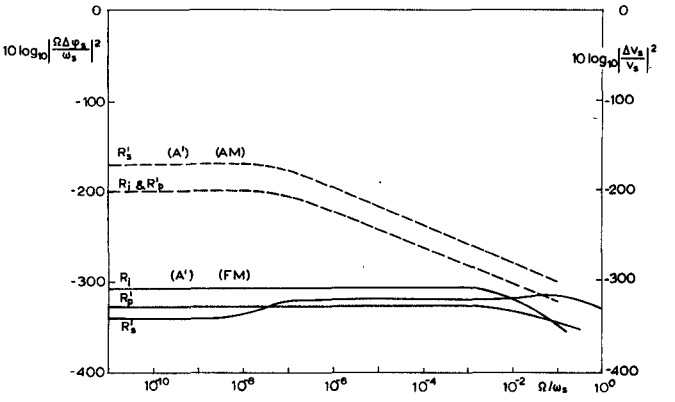

Fig. 5. Output spectral density of amplitude and phase fluctuations due to thermal noise of the pump mesh ($T_p = 300$ K), of idler spreading resistance ($T_i = 77$ K) and signal spreading resistance ($T_s = 20$ K). Continuous lines = FM noise; dashed lines = AM noise.

TABLE III
INFLUENCE OF THE BIAS VOLTAGE FLUCTUATIONS IN THE STATIC LIMIT

CASE	$20 \log_{10} \left\| \frac{\Omega \Delta\varphi_s/\omega_s}{\Delta v_b/v_{b0}} \right\|$	$20 \log_{10} \left\| \frac{\Delta v_s/v_{s0}}{\Delta v_b/v_{b0}} \right\|$
(A') (A")	- 126	- 132
(B)	- 137	- 1
(C)	- 146	5

obtained as

$$\lim_{\Omega \to 0} \left| \frac{\Delta v_s/v_{s0}}{\Delta v_g/v_{g0}} \right| = \frac{R_g}{R_g - R'_p}.$$

The effects of bias voltage fluctuations on the output signal are reported, in the static limit, in Table III. Only these data have been computed since, in (6), the bypass circuit for the bias generator was not included.

In Fig. 5, the effects of thermal noise in one of the maximum efficiency conditions are shown for the temperature values indicated. For the other operating conditions some improvement has been found both in the AM and in the FM output spectra.

Change in the steady-state operation and in another noise source, not included in the previous equation (3), are due to the nonlinear surface impedance of the superconducting output cavity. The frequency shift caused by the London penetration depth easily can be taken into account with an appropriate value of the output circuit reactances. The AM–FM fluctuations caused by the nonlinear surface reactance can be evaluated on the basis of Halbritter's work [10], and turn out to be negligible with respect to the main noise sources already reported.

V. FREQUENCY STABILITY PERFORMANCE EVALUATION

In the preceding sections, a careful analysis of a parametric oscillator using an abrupt junction varactor with fixed bias has been carried out. It includes not only the

static behavior, but also the dynamical fluctuations. Since most of the practical interest of such devices regards the realization of sources having very high stability in the short and medium term, it is interesting at this point to evaluate the overall stability performance that can be expected on the basis of the theory previously developed.

The evaluation of the oscillator stability, in the frequency domain, is performed by considering the power spectral density of the output phase fluctuations $S_\Phi(f)$ expressed in decibels. This quantity can be computed by taking into consideration the following contributions: amplitude and phase fluctuations of the pump generator, bias voltage source instability, and thermal noise. The numerical evaluations have been carried out with reference to the oscillator already examined in Sections III and IV, that is, pump frequency 20 GHz, signal frequency 11 GHz, output cavity operating at liquid He temperature with $Q_s = 10^8$, idler resonator with $Q_i = 10^2$, optimum pump power of 5 mW, and bias voltage of 1 V. A K-band pump oscillator having a good amplitude and phase spectral purity was considered; more precisely, its phase spectrum was assumed as

$$S_\Phi = \left[1.6\cdot 10^{-3} f^{-3} + 1.6\cdot 10^{-11}\right] \text{rad}^2\cdot\text{Hz}^{-1}, \quad f \lesssim 100 \text{ kHz}$$

and spectrum of amplitude fluctuations as

$$\left(\frac{\Delta v_g(f)}{v_{g0}}\right)^2 = 6.6\cdot 10^{-16}\ \text{Hz}^{-1}, \quad f \lesssim 5 \text{ MHz}.$$

The bias voltage was supposed, due to a battery having a short-term fluctuation spectrum of

$$\left(\frac{\Delta V_b(f)}{V_{b0}}\right)^2 = 10^{-18}\ \text{Hz}^{-1}, \quad f \lesssim 100 \text{ kHz}.$$

By using these data and the results of Table III and Figs. 3, 4, and 5, the contributions to the phase spectral density of the output signal are obtained and plotted in Fig. 6. From this diagram, one can see that the most significant contribution is given by the AM–PM conversion, while the thermal noise (the only one accounted for in Stein's work [3]) is by far less important. Moreover, in the present analysis, the heaviest of the thermal noise sources is the idler one. We can also mention that the S_Φ level of all contributions is strongly dependent on Q_s (they are numerically proportional to Q_s^{-2}) and that the oscillator design for maximum efficiency does not appear as the best choice from the stability point of view.

From a similar analysis performed on the output amplitude fluctuations, it turns out that their overall spectrum is approximately -160 dB/Hz for the optimum condition (A'), while it is -166 dB/Hz for case (C) of Table II. The rolloff is determined by the signal cavity bandwidth.

The overall performance of the oscillator is summarized in Fig. 7, where the characteristic of an X-band signal obtained by direct multiplication from a highly pure 5-MHz quartz oscillator [11] is also reported, for comparison purposes.

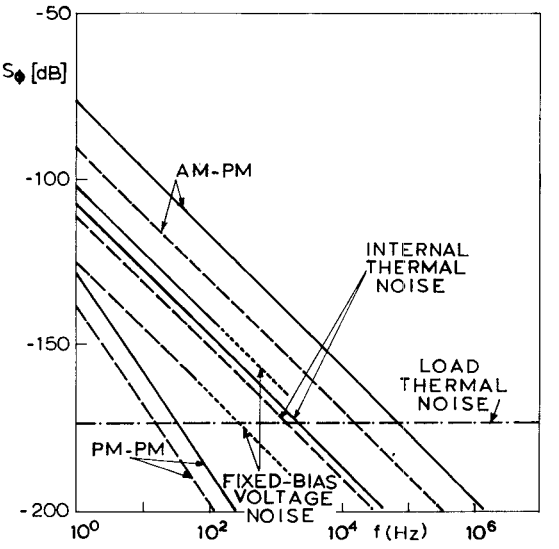

Fig. 6. Contributions to the spectral density of phase fluctuations of the output signal as a function of Fourier frequency for two operating conditions of the superconducting output cavity oscillator: maximum efficiency operation ((A') of Table II, continuous lines) and nonoptimum bias voltage operation ((C) of Table II, dashed lines).

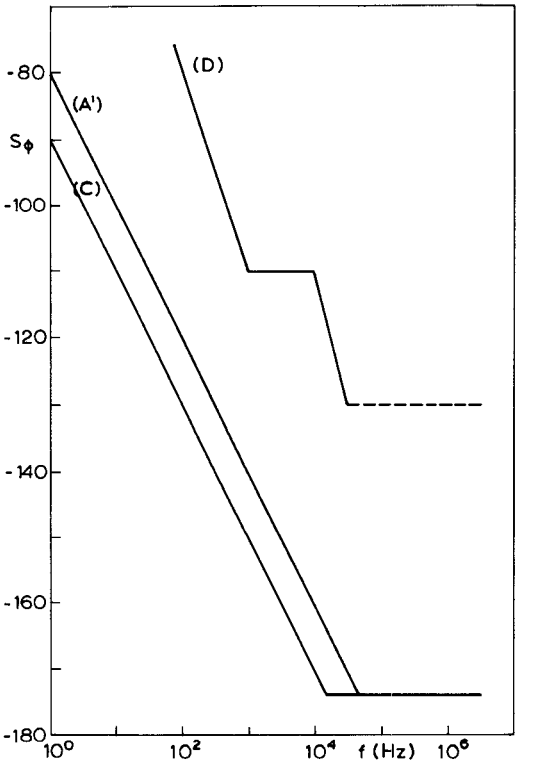

Fig. 7. Overall spectral density of phase fluctuations S_Φ as a function of Fourier frequency for the two cases (A') and (C) of Table II (parametric oscillator) and an X-band synthesized signal ((D), as obtained from a 5-MHz quartz oscillator).

In Fig. 8, the time domain stability of the parametric oscillator with superconducting cavity (obtained from the results of Fig. 7) is compared with the corresponding values of a laboratory caesium primary standard and hydrogen maser [12]. From this diagram it appears that for

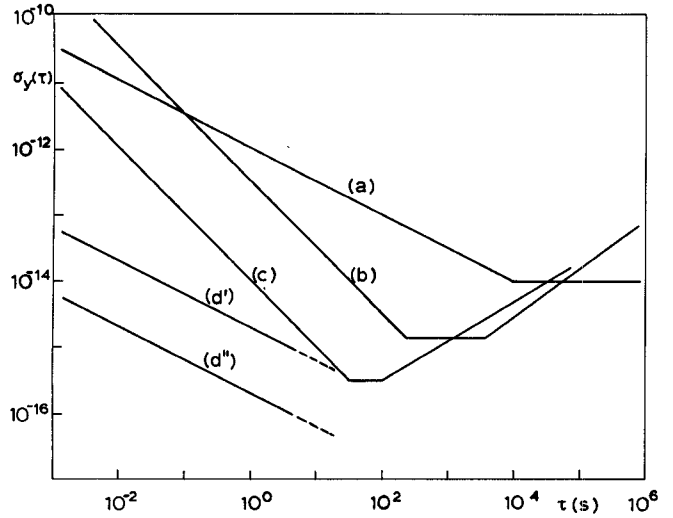

Fig. 8. Allan variance as a function of sampling time τ for various highly stable generators: *A* Laboratory Cs primary standard [12]. *B* Hydrogen maser [12]. *C* Superconducting cavity stabilized oscillator [1]. *D'*, *D''* superconducting output cavity parametric oscillator (theoretical performance) with $Q_s = 10^8$ and $Q_s = 10^9$, respectively.

observation times (τ) less than some tenths of a second, the parametric oscillator is the best frequency reference. This characteristic has already been pointed out in Stein's paper [3] but, from the analysis performed in the present paper, the advantage is not so outstanding. Moreover, some limitations due to the physical conditions of the superconducting cavity and to the refrigeration have not been considered; these effects could further reduce the stability previously evaluated.

VI. Conclusion

The analysis of a parametric oscillator model has been carried out in order to evaluate the most important contributions to amplitude and phase fluctuations.

It has been found that the main frequency instability source is the AM–PM conversion; nevertheless, a parametric oscillator with a superconducting output cavity could be the most stable source in the medium term.

This conclusion is supported by the comparison with the Cs beam standard and the H-maser performance.

Although the reported numerical results refer to a well-defined choice of circuit parameters and operation frequencies, the most important oscillator characteristics are believed not to depend substantially on the assumed numerical values.

Appendix I

The oscillator power transfer efficiency is given by

$$\eta = \frac{P_L}{P_{\text{av}}} = 4R_g R_L \frac{(\omega_s q_s)^2}{v_g^2}. \tag{A1}$$

The maximum η, for given available pump power and pump and signal frequencies, is obtained with a proper choice of R_g, R_L, and V_b. This work is analogous to that extensively performed for varactor frequency multipliers [5] and will be only briefly summarized.

A. Three-Mesh Oscillator

Input matching, for maximum η, requires

$$R_g = R_p' + \frac{mq_s q_i \cos\psi_0}{\omega_p q_p} \tag{A2a}$$

$$\varphi_p = \varphi_g \tag{A2b}$$

where in addition to the loss resistance R_p' the input resistance at the varactor terminals, as obtained from (7e), is considered in (A2a).

Combining (7) and (A2), the following expressions result:

$$\eta = \frac{\omega_s}{\omega_p} \frac{1 - R_p'/R_g}{1 + R_s'/R_L} \tag{A3a}$$

$$\cos^2\psi_0 = \frac{\omega_s \omega_i \omega_p^2}{2m^2 P_{\text{av}}} R_i R_g (R_L + R_s'). \tag{A3b}$$

The expression of η given by (A3a) has to be maximized with respect to R_g/R_p' and R_L/R_s' under the constraint

$$\psi_0 = 0 \tag{A4}$$

as we can see from (A3b).

By this way the simple expressions of Section III are obtained. Moreover, the following expressions for the charge amplitudes turn out:

$$q_p = \frac{1}{\omega_p}\sqrt{\frac{2P_{\text{av}}}{R_g}} \tag{A5a}$$

$$q_s = \sqrt{\frac{2}{\omega_s \omega_p} \frac{R_g - R_p'}{R_L + R_s'} \frac{P_{\text{av}}}{R_g}} \tag{A5b}$$

$$q_i = \sqrt{\frac{R_s \omega_s}{R_i \omega_i}} \quad q_s = \sqrt{\frac{2}{\omega_i \omega_p} \frac{R_g - R_p'}{R_i'} \frac{P_{\text{av}}}{R_g}}. \tag{A5c}$$

B. Two-Mesh Oscillator

If the idler mesh is suppressed and the output impedance Z_s allows the current to flow in a narrow band around $\omega_p/2$, a parametric frequency divider is obtained. In this case, the divider equations are obtained by neglecting (3c) and (3d), where now $\omega_s = \omega_p/2$, and replacing (5) for an abrupt junction varactor with

$$F_c^s = -mq_s q_p \cos(2\varphi_s - \varphi_p)$$

$$F_s^s = -2mq_0 q_s + mq_s q_p \sin(\varphi_p - 2\varphi_s)$$

$$F_c^p = \frac{1}{2} mq_s^2 \cos(\varphi_p - 2\varphi_s)$$

$$F_s^p = -2mq_0 q_p + \frac{1}{2} mq_s^2 \sin(\varphi_p - 2\varphi_s).$$

By means of the preceding relations and of (3), the steady-state operation of the divider is described by the

equations

$$R_s\omega_s q_s - mq_s q_p \cos\vartheta_0 = 0$$
$$-X_s\omega_s q_s - 2mq_0 q_s + mq_s q_p \sin\vartheta_0 = 0$$
$$R_p\omega_p q_p + \frac{1}{2}mq_s^2\cos\vartheta_0 = v_g\cos\varphi_0$$
$$-X_p\omega_p q_p - 2mq_0 q_p + \frac{1}{2}mq_s^2\sin\vartheta_0 = v_g\sin\varphi_0$$

where

$$\vartheta_0 = \varphi_p - 2\varphi_s \text{ and } \varphi_0 = \varphi_p - \varphi_g.$$

Obviously, the bias equation (6) still holds, with $q_i = 0$.

In the same way as before, taking into account the matching conditions, the following expression comes out:

$$\eta_d = \frac{1 - R_p'/R_g}{1 + R_s'/R_L}$$

under the constraint

$$\vartheta_0 = 0.$$

η_d is maximized by those values of R_g/R_p' and R_L/R_s' that are solutions of

$$2\left(\frac{R_L}{R_s'}\right)^3 + 5\left(\frac{R_L}{R_s'}\right)^2 + 4\left(\frac{R_L}{R_s'}\right) + 1 - \frac{1}{k_d} = 0$$

$$\frac{R_g}{R_p'} = \frac{1}{k_d\left(\frac{R_L}{R_s'} + 1\right)^2}$$

where

$$k_d = \frac{(\omega_s\omega_p)^2 R_p' R_s'^2}{2m^2 P_{\text{av}}}.$$

Since it must be $k_d \leqslant 1$ to get positive real solutions, a threshold condition similar to that given by (12) can be obtained.

Once the characteristics of the signal resonator are known, then the same considerations of Section III with respect to X_p, q_0, and V_b apply.

Appendix II

According to the hypothesis of Section IV the fluctuations in the amplitudes (Δq_n) and phases ($\Delta\varphi_n$) of the charges Q_n' and of $q_0(\Delta q_0)$ due to the pump and bias instabilities and due to thermal noise can be evaluated by the following linearized system:

$$\left[1 + 2jQ_{sL}\frac{\Omega}{\omega_s}\right]\frac{\Delta q_s}{q_0} - \frac{mq_p\cos\psi_0}{R_s\omega_s}\frac{\Delta q_i}{q_0} - \frac{mq_i\cos\psi_0}{R_s\omega_s}\frac{\Delta q_p}{q_0} + \left[j\frac{q_s}{q_0}\frac{\Omega}{\omega_s} - Q_{sL}\frac{q_s}{q_0}\left(\frac{\Omega}{\omega_s}\right)^2 - \frac{mq_i q_p\sin\psi_0}{R_s\omega_s q_0}\right]\Delta\varphi_s - \frac{mq_i q_p\sin\psi_0}{R_s\omega_s q_0}\Delta\varphi_i + \frac{mq_i q_p\sin\psi_0}{R_s\omega_s q_0}\Delta\varphi_p = \frac{\sqrt{2}}{\omega_s R_s q_0}\sqrt{4kT_s R_s'} \tag{A6}$$

$$\left[j\frac{\Omega}{\omega_s} - Q_{sL}\left[1 + \left(\frac{\Omega}{\omega_s}\right)^2\right] - \frac{2mq_0}{R_s\omega_s}\right]\frac{\Delta q_s}{q_0} + \frac{mq_p\sin\omega_0}{R_s\omega_s}\frac{\Delta q_i}{q_0} + \frac{mq_i\sin\psi_0}{R_s\omega_s}\frac{\Delta q_p}{q_0} - \frac{2mq_s}{R_s\omega_s}\frac{\Delta q_0}{q_0} - \left[2jQ_{sL}\frac{q_s}{q_0}\frac{\Omega}{\omega_s} + \frac{mq_i q_p\cos\psi_0}{R_s\omega_s q_0}\right]\Delta\varphi_s - \frac{mq_i q_p\cos\psi_0}{R_s\omega_s q_0}\Delta\varphi_i + \frac{mq_i q_p\cos\psi_0}{R_s\omega_s q_0}\Delta\varphi_p = \frac{\sqrt{2}}{\omega_s R_s q_0}\sqrt{4kT_s R_s'} \tag{A7}$$

$$-\frac{mq_p\cos\psi_0}{R_i\omega_i}\frac{\Delta q_s}{q_0} + \left[1 + 2jQ_{iL}\frac{\omega_s}{\omega_i}\frac{\Omega}{\omega_s}\right]\frac{\Delta q_i}{q_0} - \frac{mq_s\cos\psi_0}{R_i\omega_i}\frac{\Delta q_p}{q_0} - \frac{mq_s q_p\sin\psi_0}{R_i\omega_i q_0}\Delta\varphi_s + \left[j\frac{q_i}{q_0}\frac{\omega_s}{\omega_i}\frac{\Omega}{\omega_s} - Q_{iL}\frac{q_i}{q_0}\left(\frac{\omega_s}{\omega_i}\right)^2\left(\frac{\Omega}{\omega_s}\right)^2 - \frac{mq_s q_p\sin\psi_0}{R_i\omega_i q_0}\right]\Delta\varphi_i + \frac{mq_s q_p\sin\psi_0}{R_i\omega_i q_0}\Delta\varphi_p = \frac{\sqrt{2}}{\omega_i R_i q_0}\sqrt{4kT_i R_i'} \tag{A8}$$

$$\frac{mq_p\sin\psi_0}{R_i\omega_i}\frac{\Delta q_s}{q_0} + \left[j\frac{\omega_s}{\omega_i}\frac{\Omega}{\omega_s} - Q_{iL}\left[1 + \left(\frac{\omega_s}{\omega_i}\right)^2\right] - \frac{2mq_0}{R_i\omega_i}\right]\frac{\Delta q_i}{q_0} + \frac{mq_s\sin\psi_0}{R_i\omega_i}\frac{\Delta q_p}{q_0} - \frac{2mq_i}{R_i\omega_i}\frac{\Delta q_0}{q_0} - \frac{mq_s q_p\cos\psi_0}{R_i\omega_i q_0}\Delta\varphi_s - \left[2jQ_{iL}\frac{q_i}{q_0}\frac{\omega_s}{\omega_i}\frac{\Omega}{\omega_s} + \frac{mq_s q_p\cos\psi_0}{R_i\omega_i q_0}\right]\Delta\varphi_i + \frac{mq_s q_p\cos\psi_0}{R_i\omega_i q_0}\Delta\varphi_p = \frac{\sqrt{2}}{\omega_i R_i q_0}\sqrt{4kT_i R_i'} \tag{A9}$$

$$\frac{mq_i\cos\psi_0}{R_p\omega_p}\frac{\Delta q_s}{q_0} + \frac{mq_s\cos\psi_0}{R_p\omega_p}\frac{\Delta q_i}{q_0} + \left[1 + 2jQ_{pL}\frac{\omega_s}{\omega_p}\frac{\Omega}{\omega_s}\right]\frac{\Delta q_p}{q_0} + \frac{mq_s q_i\sin\psi_0}{R_p\omega_p q_0}\Delta\varphi_s + \frac{mq_s q_i\sin\psi_0}{R_p\omega_p q_0}\Delta\varphi_i + \left[j\frac{q_p}{q_0}\frac{\omega_s}{\omega_p}\frac{\Omega}{\omega_s} - Q_{pL}\frac{q_p}{q_0}\left(\frac{\omega_s}{\omega_p}\right)^2\left(\frac{\Omega}{\omega_s}\right)^2 - \frac{mq_s q_i\sin\psi_0}{R_p\omega_p q_0} + \frac{v_{g0}\sin\varphi_0}{R_p\omega_p q_0}\right]\Delta\varphi_p = \frac{v_{g0}\cos\varphi_0}{R_p\omega_p q_0}\frac{\Delta v_g}{v_{g0}} + \frac{v_{g0}\sin\varphi_0}{R_p\omega_p q_0}\Delta\varphi_g + \frac{\sqrt{2}}{\omega_p R_p q_0}\sqrt{4kT_p R_p} \tag{A10}$$

$$\left[\frac{mq_i\sin\psi_0}{R_p\omega_p}\frac{\Delta q_s}{q_0}+\frac{mq_s\sin\psi_0}{R_p\omega_p}\frac{\Delta q_i}{q_0}+\left[j\frac{\omega_s}{\omega_p}\frac{\Omega}{\omega_s}-Q_{pL}\cdot\left[1+\left(\frac{\omega_s}{\omega_p}\right)^2\left(\frac{\Omega}{\omega_s}\right)^2\right]-\frac{2mq_0}{R_p\omega_p}\right]\frac{\Delta q_p}{q_0}-\frac{2mq_p}{R_p\omega_p}\frac{\Delta q_0}{q_0}-\frac{mq_iq_s\cos\psi_0}{R_p\omega_pq_0}\Delta\varphi_s-\frac{mq_iq_s\cos\psi_0}{R_p\omega_pq_0}\Delta\varphi_i+\left[\frac{mq_iq_s\cos\psi_0}{R_p\omega_pq_0}-2jQ_{pL}\frac{q_p}{q_0}\frac{\omega_s}{\omega_p}\frac{\Omega}{\omega_s}-\frac{v_{g0}\cos\varphi_0}{R_p\omega_pq_0}\right]\Delta\varphi_p=\frac{v_{g0}\sin\varphi_0}{R_p\omega_pq_0}\frac{\Delta v_g}{v_{g0}}-\frac{v_{g0}\cos\varphi_0}{R_p\omega_pq_0}\Delta\varphi_g+\frac{\sqrt{2}}{\omega_pR_pq_0}\sqrt{4kT_pR_p}\right. \tag{A11}$$

$$\left[\frac{q_s}{q_0}\frac{\Delta q_s}{q_0}+\frac{q_i}{q_0}\frac{\Delta q_i}{q_0}+\frac{q_p}{q_0}\frac{\Delta q_p}{q_0}+2\frac{\Delta q_0}{q_0}=\frac{V_{b0}}{mq_0^2}\frac{\Delta V_b}{V_{b0}}\right. \tag{A12}$$

where $q_n, \psi_0, \varphi_0, v_{g0}, V_{b0}$ define the static working point and "Δ" accounts for the deviations from such a condition; $Q_{nL}=\omega_nL_n/R_n$, k is Boltzmann's constant, and T_n are the absolute temperatures of the corresponding resistances. Obviously, since the different noise sources are uncorrelated, their power contributions at the output must be evaluated separately and then added.

It can be observed that the current phase fluctuations $\Delta\varphi_s$, $\Delta\varphi_i$, and $\Delta\varphi_p$ are independent variables in the system (A6)–(A12) whereas in the steady-state operation only the phase differences ψ_0 and φ_0 are independent.

The known terms of the system (A6)–(A12) account for pump and bias voltage fluctuations and thermal noise of the circuit loss resistance. The transfer functions for amplitude and phase fluctuations and the additive noise contribution of the parametric oscillator have been computed by solving the system (A6)–(A12) numerically, and typical results are discussed in Section IV.

References

[1] S. R. Stein and J. P. Turneaure, "Superconducting-cavity stabilized oscillators with improved frequency stability," *Proc. IEEE*, pp. 1249–1250, Aug. 1975.

[2] S. R. Stein, "Application of superconductivity to precision oscillators," in *Proc. 29th Annual Symp. Frequency Control* (Atlantic City, NJ), May 28–30, 1975, pp. 321–327.

[3] ——, "A superconducting parametric oscillator for use in infrared frequency synthesis," in *Proc. 2nd Frequency Standards and Metrology Symp.* (Copper Mountain, CO), July 5–7, 1976, pp. 479–488.

[4] L. A. Blackwell and K. L. Kotzebue, *Semiconductor-Diode Parametric Amplifiers*. Englewood Cliffs, NJ: Prentice-Hall, 1961, pp. 101–107

[5] E. Bava, G. P. Bava, A. Godone, and G. Rietto, "Analysis of varactor frequency multipliers: Nonlinear behavior and hysteresis phenomena," *IEEE Trans. Microwave Theory Tech.*, vol. MTT-27, pp. 141–147, Feb. 1979.

[6] M. Uenohara, "Cooled varactor parametric amplifiers," in *Advances in Microwaves*, vol. 2, Leo Young, Ed. New York: Academic Press, 1967, pp. 89–164.

[7] M. Uenohara and J. W. Gewartowski, "Varactor applications," in *Microwave Semiconductor Devices and Their Circuit Applications*, H. A. Watson, Ed. New York: McGraw-Hill, 1969, ch. 8, pp. 194–270.

[8] K. Kurokawa, *An Introduction to the Theory of Microwave Circuits*. New York: Academic Press, 1969, ch. 8.

[9] A. Ralston and P. Rabinowitz, *A First Course in Numerical Analysis*, Int. Student Edition. Kogakusha, ITD: McGraw-Hill, 1978, pp. 359–367.

[10] J. Halbritter, "Change of eigenstate in a superconducting rf. cavity due to a nonlinear response," *J. Appl. Phys.*, vol. 41, no. 11, pp. 4581–4588, 1970.

[11] A. De Marchi, A. Godone, and E. Bava, "Phase coherent synthesis and precision measurements in the far-infrared," *IEEE Trans. Instrum. Meas.*, vol. IM-30, pp. 132–138, June 1981.

[12] M. Arditi, "Frequency standards: Optically pumped microwave devices," in *Metrology and Fundamental Constants*, Sc. Int. di Fisica "E. Fermi" LXVIII Corso. Società Italiana di Fisica (Bologna, Italy), pp. 289–334, 1980.

Roberto Cazzola was born in Alessandria, Italy, on July 4, 1957. He received the Dr. Ing. degree in electronic engineering from the Politecnico di Torino, Torino, Italy, in 1982.

He was engaged in research about parametric oscillation with the microwave group of the Istituto Elettrotecnico Nazionale Galileo Ferraris di Torino, Italy, in connection with his degree thesis. He was also concerned with the electromagnetic coupling between submillimetric radiation and semiconductor devices.

Gianpiero P. Poncino was born in Alessandria, Italy, in 1957. In 1982 he received the degree in electronic engineering from the Politecnico di Torino, Italy.

He was interested in parametric oscillations and in electromagnetic problems of semiconductor devices during his work for the degree thesis developed at the Istituto Elettrotecnico Nazionale Galileo Ferraris in Torino. At present he works as a software development engineer at Digital Electronic Automation, Torino, Italy.

Elio Bava was born in 1940. He received the degree in electronic engineering from the Politecnico di Torino, Torino, Italy, in 1964.

In 1966 he joined the Istituto Elettrotecnico Nazionale "Galileo Ferraris", Torino, where, for a few years, he was involved in satellite communication research. Afterwards he was mainly concerned with microwave metrology, frequency multiplication, and synthesis up to the microwave and submillimetric regions, frequency stability problems of microwave sources, and far-infrared lasers. At present he is interested in infrared laser stabilization and atomic beam submillimetric frequency standards.

Aldo Godone was born in Torino, Italy, in 1949. He received the Dr. Ing. degree in electronic engineering from the Politecnico di Torino, Italy, in 1974.

Since 1974 he has been in the microwave group of the Istituto Elettrotecnico Nazionale Galileo Ferraris di Torino, Italy. His research activity is primarily concerned with frequency multiplication by harmonic generation in the microwave and in the submillimeter regions, and in infrared laser stabilization for metrological purposes.

Gian Paolo Bava was born in 1937. He received the degree in electrical engineering from the Politecnico di Torino, Italy, in 1961.

Since 1961 he has been engaged in research work at the Istituto di Elettronica e Telecomunicazioni at Politecnico di Torino and at the Istituto Elettrotecnico Nazionale Galileo Ferraris, Torino. His research activities have been primarily concerned with TWT linearization, microwave solid-state devices, microwave transistor, and MESFET characterization and amplifier design, frequency multipliers, and integrated optics. At present he holds the rank of Professor of Microwave Techniques at the Engineering Faculty of Politecnico of Torino.